

Reciprocal interactions between mtDNA and lifespan control in budding yeast

Enrique J. Garcia[†], Janeska J. de Jonge^{†,‡}, Pin-Chao Liao, Elizabeth Stivison, Cierra N. Sing, Ryo Higuchi-Sanabria[§], Istvan R. Boldogh, and Liza A. Pon^{*}

Department of Pathology and Cell Biology and Institute of Human Nutrition, College of Physicians and Surgeons, Columbia University, New York, NY 10032

ABSTRACT Loss of mitochondrial DNA (mtDNA) results in loss of mitochondrial respiratory activity, checkpoint-regulated inhibition of cell cycle progression, defects in growth, and nuclear genome instability. However, after several generations, yeast cells can adapt to the loss of mtDNA. During this adaptation, ρ^0 cells, which have no mtDNA, exhibit increased growth rates and nuclear genome stabilization. Here, we report that an immediate response to loss of mtDNA is a decrease in replicative lifespan (RLS). Moreover, we find that adapted ρ^0 cells bypass the mtDNA inheritance checkpoint, exhibit increased mitochondrial function, and undergo an increase in RLS as they adapt to the loss of mtDNA. Transcriptome analysis reveals that metabolic reprogramming to compensate for defects in mitochondrial function is an early event during adaptation and that up-regulation of stress response genes occurs later in the adaptation process. We also find that specific subtelomeric genes are silenced during adaptation to loss of mtDNA. Moreover, we find that deletion of *SIR3*, a subtelomeric gene silencing protein, inhibits silencing of subtelomeric genes associated with adaptation to loss of mtDNA, as well as adaptation-associated increases in mitochondrial function and RLS extension.

Monitoring Editor
Thomas D. Fox
Cornell University

Received: Jun 12, 2018
Revised: Sep 25, 2019
Accepted: Oct 1, 2019

INTRODUCTION

Mitochondrial DNA (mtDNA) encodes subunits of the electron transport chain and ATP synthase, as well as components required for mitochondrial protein synthesis. For example, mtDNA of the budding yeast *Saccharomyces cerevisiae* encodes protein subunits of respiratory chain complexes III, IV, V, and the mitoribosome, as well as rRNAs and tRNAs (Contamine and Picard, 2000). Although

mtDNA can be deleted in *S. cerevisiae* or in cultured mammalian cells (Nagley and Linnane, 1970; King and Attardi, 1989), it is essential in complex multicellular organisms. Indeed, mutations of human mtDNA have clinical manifestations in the brain, heart, skeletal muscle, kidney, and endocrine system (Wallace, 2005; Park and Larsson, 2011).

There are also extensive links between mtDNA and lifespan control. For example, there is an age-associated increase in oxidative damage and mutations in mtDNA and a decrease in mitochondrial respiration in humans, mice, and mammalian cells (Muller-Hocker, 1989, 1990; Muller-Hocker *et al.*, 1992; Trounce *et al.*, 1989; Mecocci *et al.*, 1993; Melov *et al.*, 1995, 1997, 1999). Moreover, *PolgA^{mut/mut}* mutator mice that carry mutations that inhibit the mtDNA proofreading activity of DNA polymerase gamma (*PolgA*) exhibit elevated levels of mtDNA mutation, premature aging, and phenotypes associated with aging in humans (Trifunovic *et al.*, 2004; Kujoth *et al.*, 2005). These findings raise the possibility that mutation of mtDNA may contribute to aging.

However, it is not clear whether mutation or loss of mtDNA function is a cause or consequence of aging. The level of mtDNA mutations in homozygous *PolgA^{mut/mut}* mice is highly variable and in some tissues more than an order of magnitude higher than that observed in aging humans (Khrapko *et al.*, 2006). Moreover,

This article was published online ahead of print in MBoc in Press (<http://www.molbiolcell.org/cgi/doi/10.1091/mbc.E18-06-0356>) on October 10, 2019.

[†]These authors made equal contributions to the manuscript.

Present addresses: [‡]Cambridge Institute for Medical Research, University of Cambridge, The Keith Peters Building, Cambridge CB2 0XY, UK; [§]Department of Molecular and Cell Biology, Howard Hughes Medical Institute, University of California, Berkeley, Berkeley, CA 94720.

*Address correspondence to: Liza A. Pon (lap5@cumc.columbia.edu).

Abbreviations used: A, early-stage adapted cells; AA, late-stage adapted cells; CLS, chronological lifespan; DHE, dihydroethidium; GO, gene ontology; mtDNA, mitochondrial DNA; *PolgA*, polymerase gamma; RIN, RNA Integrity Number; RLS, replicative lifespan; roGFP, redox-sensing variant of GFP; UA, unadapted.

© 2019 Garcia, de Jonge, *et al.* This article is distributed by The American Society for Cell Biology under license from the author(s). Two months after publication it is available to the public under an Attribution–Noncommercial–Share Alike 3.0 Unported Creative Commons License (<http://creativecommons.org/licenses/by-nc-sa/3.0>).

“ASCB®,” “The American Society for Cell Biology®,” and “Molecular Biology of the Cell®” are registered trademarks of The American Society for Cell Biology.

heterozygous PolgA^{+/mut} mice, which have lower levels of mtDNA mutations compared with homozygous PolgA^{mut/mut} mice but ~30–200 times higher than wild-type mice, do not exhibit any premature aging or reduction in lifespan (Vermulst *et al.*, 2007). Thus, while PolgA mutator mice are widely used to study diseases associated with mutations of mtDNA, it is not clear that they model the normal aging process.

Studies in budding yeast have not provided a clearer understanding of the links between mtDNA and lifespan control. Aging studies in yeast can model two distinct forms of cellular aging. Chronological lifespan (CLS), the survival time of stationary-phase, nondividing yeast cells, is a model for stress resistance in postmitotic cells (MacLean *et al.*, 2001). Replicative lifespan (RLS), the number of times that a cell can divide prior to senescence, is a model for aging of division-competent cells (Mortimer and Johnston, 1959). Budding yeast cells exhibit an increase in mutation or loss of mtDNA as they undergo replicative aging (Veatch *et al.*, 2009). On the other hand, deletion of mtDNA can result in an increase in RLS and the observed lifespan extension is not due to loss of mitochondrial respiratory activity or reduced oxidative stress in mitochondria (Woo and Poyton, 2009). However, other studies indicate that loss of mtDNA can increase, decrease, or have no effect on RLS (Kirchman *et al.*, 1999; Kaerberlein *et al.*, 2005). Thus, the link between loss of mtDNA and aging remains elusive in yeast and other eukaryotes.

We reevaluated the effect of mtDNA on yeast RLS, in part because yeast cells adapt to loss of mtDNA. The immediate response to loss of mtDNA in yeast is loss of respiratory activity, activation of the mtDNA inheritance checkpoint, reduced growth rate, and a high rate of nuclear genome instability (Slonimski *et al.*, 1968; Veatch *et al.*, 2009; Crider *et al.*, 2012). The mtDNA inheritance checkpoint inhibits progression from G₁ to S phase in response to loss of mtDNA and is regulated by Rad53p, a component of the DNA damage checkpoint signaling pathway (Crider *et al.*, 2012). The nuclear genome instability observed in cells without mtDNA (referred to as rho⁰ cells) is a consequence of decreased mitochondrial membrane potential ($\Delta\Psi$), which in turn results in defects in the formation of iron–sulfur clusters, cofactors that are essential for the normal function of proteins including those that affect nuclear genome integrity (Veatch *et al.*, 2009).

Early studies revealed that rho⁰ cells adapt to loss of the mitochondrial genome. During this process, they exhibit increased growth rates and nuclear genome stability. Adaptation to loss of mtDNA is affected by environmental factors including pH, temperature, nutrient availability, antioxidants, and coculture with cells that have mtDNA (Veatch *et al.*, 2009; Dirick *et al.*, 2014). Here, we report that loss of mtDNA results in a decrease in RLS, and that one consequence of adaptation to loss of mtDNA is an extension of RLS. Moreover, we obtained evidence for a role for subtelomeric gene silencing in the process of rho⁰ cell adaptation (Dang *et al.*, 2009). In yeast, as in other eukaryotes, telomeres act as caps at the ends of chromosomes to protect them from exonuclease degradation and end-to-end fusions. The DNA repeat TG₁₋₃ at the ends of all yeast chromosomes binds to conserved proteins that regulate telomere length, transcription, and packaging and is both necessary and sufficient to provide telomere function (Shampay *et al.*, 1984; Walmsley *et al.*, 1984; Wellinger and Zakian, 1989; Grunstein, 1997). Other studies support a role for conserved lifespan regulatory proteins in subtelomeric gene silencing. Specifically, a complex consisting of the Sirtuins Sir2p, Sir3p, and Sir4p is recruited to telomeres and subtelomeric regions, where they catalyze deacetylation of histones adjacent to the nucleosome, which leads to chromatin condensation and gene silencing (Park and Lustig, 2000; Rusche *et al.*, 2003;

Altaf *et al.*, 2007; Dang *et al.*, 2009; Kozak *et al.*, 2010). We find that specific subtelomeric genes are silenced in yeast as they adapt to loss of mtDNA, and that Sir3p is required for silencing of at least three different subtelomeric genes, as well as for improved mitochondrial function and RLS extension during this adaptation process.

RESULTS AND DISCUSSION

Yeast adapt to loss of mtDNA

We confirmed previous findings (Veatch *et al.*, 2009; Dirick *et al.*, 2014) that rho⁰ cells adapt to loss of mtDNA. Freshly prepared rho⁰ cells form small and large colonies on solid media (Figure 1, A and B). Cells from both small and large rho⁰ cell colonies have no respiratory activity and grow significantly more slowly than rho⁺ cells, which contain mtDNA (Figure 1C). However, cells from large rho⁰ colonies exhibit higher growth rates than cells from small rho⁰ colonies (Figure 1C). It is likely that the large colonies represent a population of rho⁰ cells that have adapted to the loss of mtDNA and thus exhibit faster growth rates. Therefore, we will refer to the cells from small and large colonies of rho⁰ strains as unadapted (UA) and adapted, respectively.

Interestingly, we find that UA rho⁰ cells give rise to cells that form small colonies and exhibit low growth rates, but they also give rise to cells that form large colonies and exhibit high growth rates. Thus, UA rho⁰ cells give rise to both UA and adapted rho⁰ cells. In contrast, adapted rho⁰ cells give rise only to adapted cells, which form large colonies and exhibit high growth rates (Figure 1, A–C). These data confirm previous findings that the adaptation observed in rho⁰ cells is heritable (Dirick *et al.*, 2014). Moreover, rho⁰ cells continue to adapt as they are propagated. We find that the colonies produced from adapted rho⁰ cells are significantly larger than those obtained from newly generated rho⁰ cells (Figure 1B).

Our initial observation of rho⁰ adaptation was made in cells where mtDNA was eliminated by treatment with EtBr. However, we also observe adaptation in rho⁰ cells in which mtDNA has been lost as a result of the deletion of *MGM101* (Supplemental Figure S1), which encodes a protein that mediates mtDNA repair and is required for mtDNA maintenance (Chen *et al.*, 1993). Adaptation to loss of mtDNA has also been documented in yeast that undergo spontaneous mtDNA loss and in yeast in which mtDNA loss was induced by expression of a dominant-negative form of the mtDNA polymerase *MIP1* (Veatch *et al.*, 2009; Dirick *et al.*, 2014). Thus, this adaptation is a general response to loss of mtDNA and not a consequence of the method used to delete mtDNA. The collective findings that yeast cells adapt to loss of mtDNA raise the possibility that mammalian rho⁰ cells can also adapt to loss of mtDNA.

Finally, we find that the increase in growth rate that occurs in adapted rho⁰ colonies is due at least in part to bypass of the mtDNA inheritance checkpoint (Figure 1D). We monitored cell cycle progression in synchronized yeast cells using flow cytometry to measure DNA content. Wild-type rho⁺ cells, which contain mtDNA, transition from G₁ to G₂ phase 60–130 min after release from G₁ arrest. In contrast, cells from small rho⁰ colonies exhibit severe defects in transition from G₁ to S phase. Finally, cells from large rho⁰ colonies progress through the cell cycle similarly to rho⁺ cells. In the example shown, the lag time for entry into the cell cycle after release from G₁ arrest and the cycling times are shorter in adapted rho⁰ cells than in rho⁺ cells.

Effects of mtDNA on lifespan and mitochondrial redox state

One consequence of loss of mtDNA and the associated mitochondrial respiratory activity is a decrease in $\Delta\Psi$. Previous studies

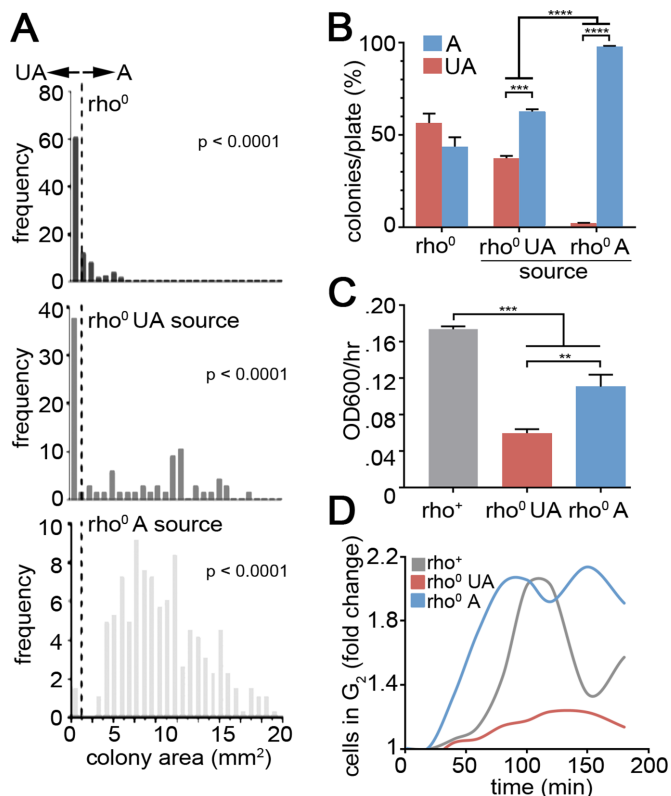


FIGURE 1: Yeast adapt to loss of mtDNA. (A) Distribution of yeast colony area from rho⁰ (newly generated rho⁰ cells), rho⁰ UA source (rho⁰ cells derived from UA small rho⁰ colonies), and rho⁰ A source (rho⁰ cells derived from adapted large rho⁰ colonies). Representative trial from three independent experiments. The dotted line indicates colony area threshold criterion used to define adapted colonies. The *p* values indicate statistically significant differences between the average colony sizes of the strains (*n* = 137–322 colonies measured per condition; *****p* < 0.0001, by Kruskal–Wallis test with Dunn’s post-hoc test for multiple comparisons). (B) The percentage of UA and adapted colonies, according to colony area criteria used in A, from newly generated rho⁰, rho⁰ UA, and rho⁰ A sources. The bar represents the average percentage of colonies of each size ± SEM in three independent experiments (*n* = 68–322 colonies per experiment per condition; ****p* < 0.001; and *****p* < 0.0001, by one-way ANOVA with Tukey post-hoc test). (C) Growth rates of rho⁺, rho⁰ UA, and rho⁰ A cells. The bar shows pooled average ± SEM of the maximum OD₆₀₀/h from three independent experiments (*n* = 6–12 replicates per conditions; ***p* < 0.01; and ****p* < 0.001, by one-way ANOVA with Tukey post-hoc test). (D) Quantitation of progression from G₁ to G₂ for rho⁺, rho⁰ UA, and rho⁰ A cells. Cells were incubated with mating pheromone (alpha factor), which arrests cells in the G₁ phase of the cell cycle. Progression of cells from G₁ to G₂ stages of the cell cycle was monitored after release from G₁ using flow cytometry to measure the levels of propidium iodide stained DNA. Progression was measured as the fold change in the fraction of cells in G₁ phase at the time specified, relative to the fraction of cells that were in G₁ at the time of release from alpha factor-induced G₁ arrest (cells in G₁ at t₀/cells in G₁ at t_x, 50,000 events measured per timepoint per strain).

revealed that $\Delta\Psi$ increases as yeast adapt to loss of mtDNA (Veatch et al., 2009). To further characterize the adaptation process, we studied mitochondrial redox state in UA and adapted rho⁰ cells using a redox-sensing variant of GFP (roGFP) (Figure 2, A and B) (Hanson et al., 2004). Our previous studies using mitochondria-targeted roGFP and other biosensors revealed that fitter mitochondria

that are more reduced, contain less mitochondrial superoxide, and have higher $\Delta\Psi$ are preferentially inherited by yeast daughter cells and that this affects yeast cell fitness and lifespan (McFaline-Figueroa et al., 2011).

Loss of mtDNA or adaptation to that loss does not affect mitochondrial quality control during inheritance: daughter cells inherit mitochondria that are more reduced and therefore higher functioning in adapted and UA rho⁰ cells (Supplemental Figure S2). However, mitochondria in UA rho⁰ cells are significantly more oxidized compared with mitochondria in rho⁺ cells. Moreover, mitochondrial redox state improves in rho⁰ cells as they adapt. Here, we evaluated mitochondrial redox state during early and later stages of adaptation (3 and 5 d after deletion of mtDNA, respectively). We detect a subtle but statistically significant increase in the reducing potential of mitochondria during early stages of adaptation. Furthermore, mitochondrial reducing potential continues to increase during late stages of adaptation, approaching levels observed in rho⁺ cells (Figure 2, A and B).

Interestingly, the more reducing mitochondrial environment observed on adaptation of rho⁰ cells is not accompanied by lower mitochondrial superoxide levels. Using dihydroethidium (DHE) to detect superoxides in living yeast cells, we confirmed our previous findings that all detectable superoxides in yeast colocalize with mitochondria (McFaline-Figueroa et al., 2011). Beyond this, we find that deletion of mtDNA results in loss of all detectable superoxides in mitochondria and that mitochondrial superoxide levels do not change as cells adapt to loss of mtDNA. (Supplemental Figure S2).

Thus, we detect two additional events that occur during adaptation to loss of mtDNA: bypass of the mtDNA inheritance checkpoint and improved mitochondrial redox state. Interestingly, loss of mtDNA has no effect on the mitochondrial quality control mechanisms that promote inheritance of higher-functioning mitochondria by yeast daughter cells (McFaline-Figueroa et al., 2011). Moreover, since loss of mtDNA results in loss of all detectable mitochondrial ROS, a phenotype that is stable during rho⁰ cell adaptation, mitochondrial ROS is therefore not responsible for changes in the redox state of the organelle as rho⁰ cells adapt.

Equally important, we find that rho⁰ cells undergo an extension of RLS as they adapt (Figure 2, C–E). The mean RLS of rho⁺ cells in the genetic background used in these studies is 20–25 generations. The RLS of UA and adapted rho⁰ cells is variable. However, the mean RLS of UA rho⁰ cells is always significantly lower than that of rho⁺ cells, and the generation time of UA rho⁰ cells is longer. In contrast, the mean RLS of adapted rho⁰ cells is higher than that of UA rho⁰ cells (unpublished data). In the example shown, the RLS of the adapted rho⁰ cells is greater than that of rho⁺ cells.

Thus, we detect reciprocal interactions between mtDNA and lifespan in budding yeast. Loss of mtDNA results in reduced RLS. Conversely, RLS extension is one consequence of the adaptation of yeast to loss of mtDNA. Our findings provide evidence for a role for mtDNA in lifespan control in yeast and raise the possibility that loss of mtDNA or mtDNA function may also affect lifespan in other eukaryotes. Collectively, our findings reconcile previous observations that loss of mtDNA has diverse effects on RLS in yeast: the variable RLS observed in rho⁰ cells may be a consequence of analysis of RLS in cells in different states of adaptation to loss of mtDNA.

Subtelomeric genes are silenced in adapted rho⁰ cells

Since adaptation is heritable, we used RNA-Seq to compare the transcriptomes of UA rho⁰ cells and rho⁰ cells at different stages of adaptation (Figure 3 and Supplemental Table S1). Here, we used rho⁰ cells 3 d after EtBR-mediated loss of mtDNA as a model for

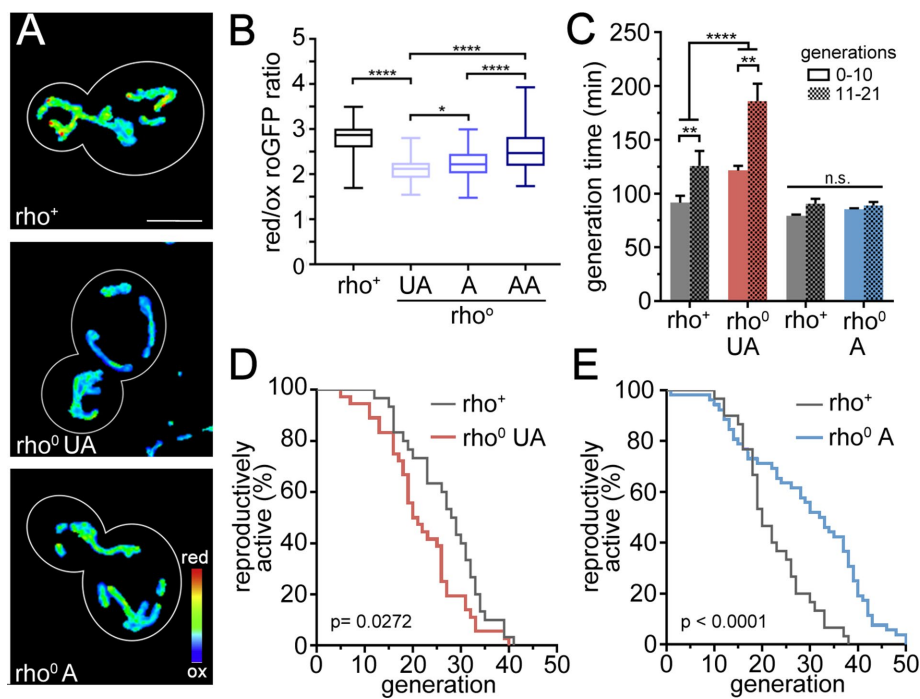


FIGURE 2: Adaptation to loss of mtDNA results in increased lifespan and mitochondrial quality. (A) Representative images of redox state of mitochondria in WT ρ^+ , ρ^0 UA, and ρ^0 A cells measured with mito-roGFP1. Reduced:oxidized mito-roGFP ratio images are shown. Color scale in the bottom panel shows the dynamic range of ratios, with warmer colors indicating a more reducing environment. (B) Quantitation of reduced:oxidized mito-roGFP ratios in WT ρ^+ , ρ^0 UA, ρ^0 A, and ρ^0 AA cells. The box indicates the middle quartile with the midline representing the median; whiskers show the minimum and maximum values. Representative trial from three independent experiments ($n = 84\text{--}104$ for each condition, $*p < 0.05$, $****p < 0.0001$, by one-way ANOVA with Tukey post-hoc test for multiple comparisons). (C) Mean generation time was measured during RLS determination shown in D and E, as the time elapsed between the emergence of two consecutive buds. Bars show average \pm SEM for one independent experiment ($n = 30\text{--}51$ cells per condition; $**p < 0.01$; and $****p < 0.0001$, by Kruskal–Wallis test with Dunn’s post-hoc test for multiple comparisons). (D, E) RLS determination for WT ρ^+ , ρ^0 UA, and ρ^0 A cells. ($n = 40\text{--}52$ starting new daughters per condition. Statistical significance between RLS survival curves was tested with Log-rank (Mantel–Cox) test where $p < 0.05$).

early-stage adaptation and ρ^0 cells >10 d after loss of mtDNA induced by deletion of *MGM101* as a model for late-stage adaptation.

We find that metabolic reprogramming to compensate for loss of mitochondrial metabolic activity occurs during early stages of adaptation in ρ^0 cells and identified biomarkers that can be used to assess ρ^0 adaptation (Figure 3 and Supplemental Table S1). Specifically, we find that pathways for amino acid and purine biosynthesis, essential functions of mitochondria, are up-regulated during early-stage adaptation in ρ^0 cells. Consistent with this, our quantitative PCR (qPCR) analysis indicates that the level of mRNA for *ADE17*, which encodes a purine biosynthetic enzyme, increases during early stages of adaptation and, during later stages of adaptation, returns to levels observed in UA ρ^0 cells (Figure 3; Supplemental Figure S3A).

In contrast, we find that oxidant stress response genes are up-regulated during late stages of adaptation (Figure 3 and Supplemental Table S1). For example, spermine is a polyamine that is induced by stressors in prokaryotes and eukaryotes, can protect DNA from oxidative damage, decreases sensitivity to oxidative stress, and has been implicated in activation of stress response gene expression (Rider *et al.*, 2007; Pegg and Michael, 2010). We find that spermine transport and biosynthesis are up-regulated during late-stage adaptation of ρ^0 cells. As described above, mitochondria

become more reducing, but we see no obvious change in mitochondrial superoxide levels during adaptation to loss of mtDNA. Therefore, it is possible that the change in mitochondrial redox state observed in adapted ρ^0 cells is due to up-regulation of spermine and other oxidant stress response factors.

It is interesting that oxidant stress response genes are up-regulated in late-stage adapted ρ^0 cells, even though there is no change in mitochondrial superoxide levels in UA and adapted ρ^0 cells. On the other hand, we detect superoxides that do not colocalize with mitochondria in UA ρ^0 cells. Therefore, it is possible that extramitochondrial ROS drives the mitochondrial antioxidant response.

Our transcriptome analysis also revealed that specific subtelomeric genes are preferentially silenced in ρ^0 cells in both early and late stages of adaptation (Supplemental Tables S1 and S2). We find that 24% of the transcripts that are down-regulated during early adaptation are encoded by genes that lie within 25 kb of the telomere and are therefore subtelomeric. Indeed, the subtelomeric genes that appear to be silenced in adapted ρ^0 cells are present in 11 of the 16 yeast chromosomes (Figure 4, A and B).

Early studies supported the model that subtelomeric silencing is a consequence of spreading of silencing mediators (e.g., the Sir2/3/4 protein complex) from telomeres to subtelomeres (Gottschling *et al.*, 1990; Renaud *et al.*, 1993). However, other studies raised questions regarding the generality of this model. Indeed, transcriptome analysis and chromatin immunoprecipitation

studies revealed that the Sir2/3/4 complex localizes to discrete, noncontinuous sites on subtelomeres and is responsible for silencing of only 6% of the genes in subtelomeres (Ellahi *et al.*, 2015). Thus, available evidence indicates that telomere positioning effects do not contribute to subtelomeric gene silencing by the Sir2/3/4 complex. Our transcriptome analysis indicates that only a limited number of genes are silenced within subtelomeres in adapted ρ^0 cells. In cases where more than one subtelomeric gene appears to be silenced, genes are discontinuous. Thus, there are no obvious telomere positioning effects in the subtelomeric gene silencing we observe in adapted ρ^0 cells.

On the other hand, many of the subtelomeric genes that are silenced during ρ^0 cell adaptation are functionally related. Previous studies indicate that newly generated ρ^0 cells exhibit a transcription signature of iron starvation (e.g., increased expression of iron transport and homeostasis proteins), which likely reflects compensatory mechanisms to promote the essential process of iron–sulfur cluster formation in mitochondria (Veatch *et al.*, 2009). We find that some of the subtelomeric genes that are silenced during early and late adaptation encode iron transport proteins. The other major class of subtelomeric genes that are silenced in both early- and late-stage adaptation are stress response genes including proteins in the seripauperin multigene family (Supplemental Tables S3 and S4).

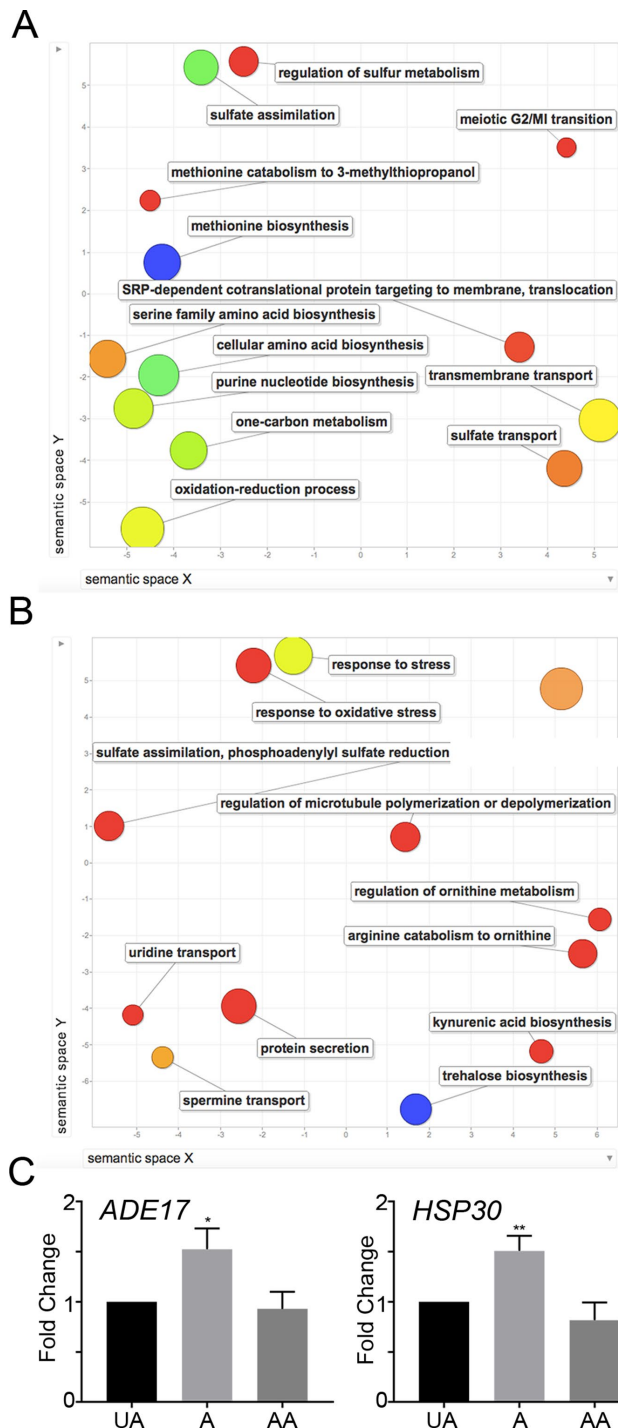


FIGURE 3: Transient up-regulation of genes occurs during adaptation to loss of mtDNA. Revigo plot of GO terms associated with genes that are up-regulated in early-stage adapted ρ^0 cells compared with UA ρ^0 cells (A) and later-stage compared with early-stage adapted ρ^0 cells (B). Bubbles with cooler colors represent more significant p values; the size of the bubble indicates the frequency of the GO term. X and Y coordinates are derived by applying multidimensional scaling to a matrix of the GO terms' semantic similarities. (C) Average fold change of transcript levels for subtelomeric genes *HSP30* and *ADE17* in early-stage adapted ρ^0 cells (A) and late-stage adapted cells (AA), relative to WT ρ^0 UA cells. Fold change was calculated as $2^{-\Delta\Delta CT}$ with actin serving as the endogenous control for each sample. Averages and SEM from $n = 3$ independent trials are shown ($*p < 0.05$, $**p < 0.001$ by one-way ANOVA with Dunnett's multiple comparisons test).

Indeed, using qPCR to quantify cellular mRNA levels, we confirmed that the transcripts of two seripauperin family proteins (*PAU24* and *DAN1*) and one iron transport gene (*FIT3*) that are silenced in adapted ρ^0 cells based on RNA-Seq analysis are present in reduced levels in adapted compared with UA ρ^0 cells (Figure 4C; Supplemental Figure S3B). Importantly, these genes are silenced during both early and later stages of adaptation, indicating that subtelomeric silencing is involved in the regulation of adaptation.

SIR3 is required for adaptation to loss of mtDNA

To determine whether adaptation to loss of mtDNA is due to subtelomeric silencing, we studied the effect of deletion of *SIR3* on adaptation in ρ^0 cells. We deleted mtDNA in *sir3 Δ* cells and found that *sir3 Δ* ρ^0 cells form large and small colonies when propagated on solid media. We also find that small *sir3 Δ* ρ^0 cell colonies give rise to large and small colonies, while large *sir3 Δ* ρ^0 cell colonies give rise primarily to large colonies (Figure 5A). Thus, *sir3 Δ* ρ^0 cells have the capacity to adapt to loss of mtDNA.

However, we find that *sir3 Δ* ρ^0 cells exhibit a fundamentally different adaptation phenotype compared with ρ^0 cells that contain wild-type *SIR3*. First, in contrast to adapted ρ^0 cells, which exhibit higher rates of growth in liquid media compared with UA ρ^0 cells, the growth rate of cells from large *sir3 Δ* ρ^0 cell colonies in liquid media is significantly lower than that of UA *sir3 Δ* ρ^0 cells (Figure 5B; Supplemental Figure S4A). Although it seems counterintuitive that cells from large *sir3 Δ* ρ^0 colonies exhibit lower growth rates compared with cells from small *sir3 Δ* ρ^0 colonies, there is a precedent for differential yeast growth rates on solid versus liquid media. For example, yeast bearing a deletion in one of the *FLO* genes, which are required for adhesion (flocculation) of yeast cells, exhibit increased colony size on solid media as well as a severe reduction in growth rate in liquid media compared with wild-type cells (e.g., Di Gianvito *et al.*, 2017). Indeed, since genes that affect cell wall mannoproteins are silenced during adaptation to loss of mtDNA, it is possible that the large colony size of some *sir3 Δ* ρ^0 cells is due to effects on yeast cell adhesion.

Equally important, we detect a statistically significant decrease in the silencing rate of three subtelomeric genes (*FIT3*, *DAN1*, and *PAU24*) in *sir3 Δ* ρ^0 cells compared with ρ^0 cells during the adaptation process (Figure 5C; Supplemental Figure S4B). In addition, there is no detectable increase in mitochondrial reducing potential during adaptation of *sir3 Δ* ρ^0 cells (Figure 5, D and E). Finally, we find that the RLS of cells from adapted and UA *sir3 Δ* ρ^0 cell colonies is indistinguishable. Thus, there is no improvement in mitochondrial redox state or extension of RLS in adapted *sir3 Δ* ρ^0 cells (Figure 5F).

Our findings support the model that Sir3p-dependent subtelomeric gene silencing is responsible for improved mitochondrial function and extended RLS associated with adaptation to loss of mtDNA. While it is not clear whether the increase in mitochondrial redox state is causative in the RLS-adaptive phenotype, our previous studies (Higuchi *et al.*, 2013) indicate that rendering mitochondria more reducing is sufficient to extend RLS in yeast. Thus, it is possible that the lifespan extension observed in yeast that adapt to loss of mtDNA is due to the change in mitochondrial redox state.

Previous studies revealed a role for lifespan-regulating genes in ρ^0 cell survival. Most yeast strains can tolerate loss of mtDNA. However, yeast carrying certain mutations (e.g., mitochondrial protein import or protein quality control) require mtDNA for survival (Dunn and Jensen, 2003; Senapin *et al.*, 2003). Interestingly, deletion of conserved lifespan-regulating genes can suppress the

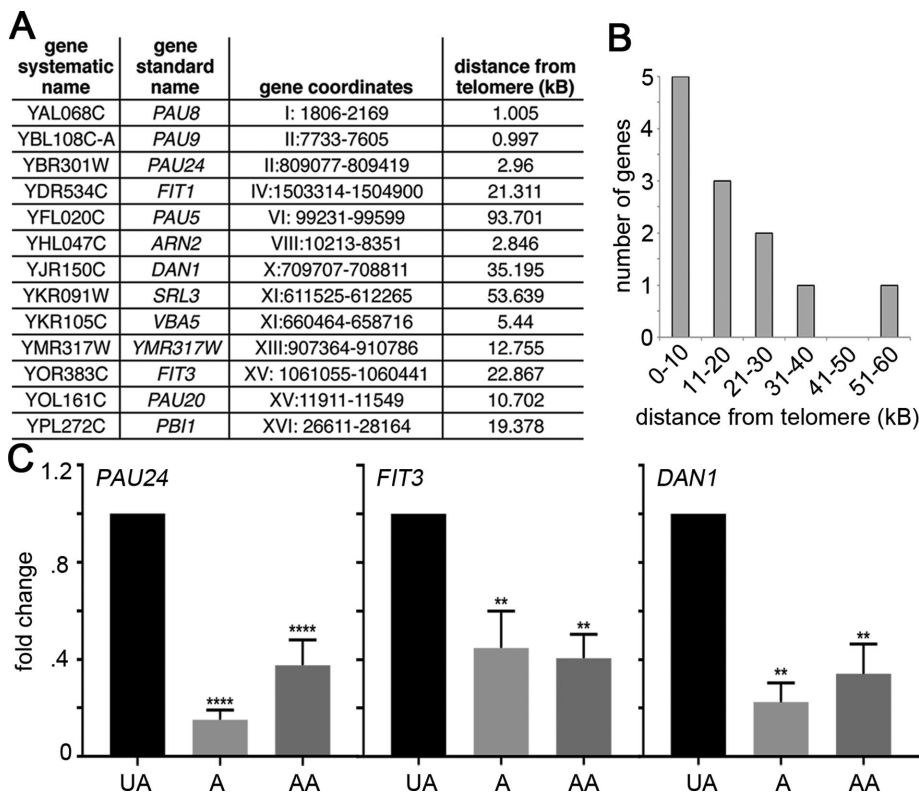


FIGURE 4: Subtelomeric gene silencing occurs during adaptation to loss of mtDNA. (A) The most down-regulated genes in early stage (A) vs. UA ρ^0 cells, listed according to their chromosomal loci. Down-regulated genes were defined as those exhibiting a Log_2 fold change < -1.5 and statistical significance of $p < 0.05$. Distance from telomere denotes the distance from the gene locus to the closest telomere in the chromosome. (B) Histogram showing distribution of distances from nearest telomere of the 13 most down-regulated genes shown in A. One gene with a distance of 93 kb is not shown. (C) Average fold change of transcript levels for subtelomeric genes *PAU24*, *DAN1*, and *FIT3* in early-stage adapted ρ^0 (A), and late-stage adapted cells (AA), compared with WT ρ^0 UA. Fold change was calculated as $2^{-\Delta\Delta\text{CT}}$ with actin serving as the endogenous control for each sample. Averages and SEM from $n = 3$ independent trials are shown (** $p < 0.01$, **** $p < 0.0001$ by one-way ANOVA with Dunnett's multiple comparisons test).

lethality observed on loss of mtDNA in these “petite-negative” strains. Specifically, deletion of any of several proteins in the 60S ribosomal subunit (*rpl13a*, *37b*, *12a*, *20b*, *19a*, *6b*, *14a*, *43b*, *34b*, *35b*, and *12b* as well as *rpp1b* and *4a*) can extend lifespan and suppress the lethality of loss of mtDNA in petite-negative yeast (Dunn et al., 2006). We do not detect changes in the levels of the transcripts of any of these RLS-extending genes. Thus, the lifespan extension observed in adapted ρ^0 cells is not due to alterations in the expression of ribosomal genes that affect ρ^0 cell viability.

Previous studies also revealed that elevated mitochondrial ROS results in extension of CLS in yeast. The extended CLS observed in these studies is a consequence of Rad53p-dependent silencing of the DNA demethylase Rph1p and the resulting increase in subtelomeric gene silencing by Sir3p (Schroeder et al., 2013). While the lifespan extension observed in yeast exposed to elevated mitochondrial ROS and in yeast that are adapting to loss of mtDNA are both Sir3p-dependent, there is evidence that these processes are mechanistically distinct. First, yeast undergoing chronological and replicative aging are in different stages of the yeast life cycle. Chronological aging occurs in yeast that have encountered nutrient limitations and/or accumulation of damaging metabolites and

cannot undergo cell division. In contrast, yeast undergoing replicative aging are cell division-competent and not nutrient-limited. Second, there is no detectable mitochondrial superoxide in UA ρ^0 cells or adapted ρ^0 cells at any stage of adaptation. Third, with the exception of one gene, there is no overlap between the 43 genes that are repressed in stationary-phase yeast with elevated mitochondrial ROS and the 42 genes that are down-regulated in early-stage adapted (A) ρ^0 cells, or the 93 genes that are repressed in later-stage adapted (AA) ρ^0 cells. Indeed, the genes that are down-regulated in adapted ρ^0 cells are different from the genes that undergo Sir2/3/4-dependent down-regulation in ρ^+ cells (Ellahi et al., 2015). Finally, we find that silencing of the three subtelomeric genes analyzed that are down-regulated in adapted ρ^0 cells does not require *RPH1* (unpublished data). These findings provide additional support for the notion that differential Sir3p-dependent subtelomeric gene silencing events occur in response to different environmental or cellular conditions. That is, Sir3p regulates different genes in dividing ρ^+ cells in oxidatively stressed quiescent ρ^+ cells and in ρ^0 cells that are adapting to loss of mtDNA.

Overall, our studies reveal new links between mtDNA and lifespan control. Loss of mtDNA results in reduced RLS. On the other hand, extension of RLS is one consequence of adaptation to loss of mtDNA. We also identified distinct transcriptome signatures during early and late stages of adaptation to loss of mtDNA. Metabolic programming to compensate for loss of key mitochondrial functions occurs early in the adaptation

process while up-regulation of specific stress response genes occurs later in that process. Finally, we find that silencing of some subtelomeric genes occurs during early and later stages of adaptation and obtained evidence for a role for Sir3p in this process and for improved mitochondrial function and extended RLS during ρ^0 cell adaptation. Ongoing studies focus on the gene(s) responsible for the RLS extension that occurs during adaptation to loss of mtDNA and how those genes contribute to that process.

MATERIALS AND METHODS

Yeast strains and growth conditions

All *S. cerevisiae* strains used in this study are derivatives of the wild-type BY4741 strain (*MATa his3 Δ 1 leu2 Δ 0 met15 Δ 0 ura3 Δ 0*) from Open Biosystems (Huntsville, AL). Yeast cells were cultivated and manipulated as described previously (Sherman, 2002). The ρ^0 cells were generated by treatment with EtBr as described in Fox et al. (1991). Briefly, each strain was grown in SC containing 25 $\mu\text{g}/\text{ml}$ ethidium bromide (EtBr; Sigma, St. Louis, MO) for 48 h at 30°C with shaking at 220 rpm. Then cells were spread on YPD and incubated for 5 d at 30°C. The ρ^0 status was confirmed by lack of growth on plates containing a nonfermentable carbon source and an absence of mtDNA by DAPI (4',6-diamidino-2-phenylindole) staining.

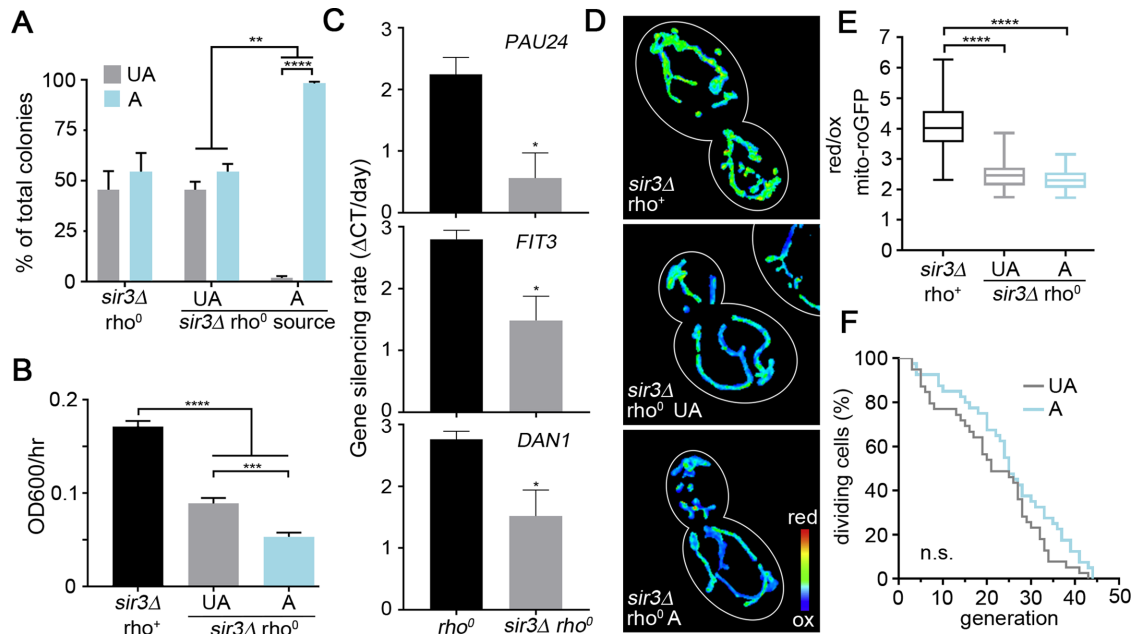


FIGURE 5: Sir3p is required for efficient adaptation to loss of mtDNA. (A) Percentage of UA and A colonies, according to colony area criteria used in Figure 1A, arising from newly generated *sir3Δ rho⁰* and from UA and adapted colonies propagated from newly generated *sir3Δ rho⁰* cells. The bar shows the average percentage distribution of colony sizes \pm SEM of three independent experiments ($n = 85\text{--}394$ per condition per experiment; $**p < 0.01$, and $****p < 0.0001$ by one-way ANOVA with Tukey post-hoc test). (B) Growth rates of *sir3Δ rho⁺* cells and cells from UA (gray column) and adapted (A, light blue) *sir3Δ rho⁰* colonies. Bars show pooled average \pm SEM of maximum OD₆₀₀/h from three independent experiments ($n = 6\text{--}12$ replicates per conditions; $***p < 0.001$ and $****p < 0.0001$, by one-way ANOVA with Tukey post-hoc test). (C) Gene silencing rate changes were determined by the change in Δ Ct between 3 and 5 d of adaptation for *PAU24*, *DAN1*, and *FIT3* in *rho⁰* and *sir3Δ rho⁰* cells. Averages and SEM from $n = 3$ independent trials are shown ($*p < 0.05$, by Student's *t* test). (D) Representative images of redox state of mitochondria measured with mito-roGFP1 in *sir3Δ rho⁺* cells, and in *sir3Δ rho⁰* cells from UA and adapted (A) colonies. (E) Quantitation of reduced:oxidized mito-roGFP ratios in *sir3Δ rho⁺* cells, and *sir3Δ rho⁰* cells from UA and A colonies. Box and whiskers are defined as in Figure 2 ($n = 48\text{--}89$ for each condition; $****p < 0.0001$, by one-way ANOVA with Tukey post-hoc test). (F) RLS measurements for *sir3Δ rho⁰* UA and A cells performed as described in *Materials and Methods* ($n = 40$ new daughters observed per condition per RLS experiment. Statistical significance between RLS survival curves was tested with Log-rank (Mantel-Cox) where $p < 0.05$).

For some studies, *rho⁰* cells were generated by replacing *MGM101* in *rho⁺* cells with knockout cassettes containing the selectable marker *LEU2* through homologous recombination according to previously described protocols (Longtine *et al.*, 1998; Gauss *et al.*, 2005). The primers, 5' CTAAAAAGGAAAGAAAGGACAAGTAGGAAGATCAGCGTACGTGCAGGTGCGACAACCCCTTAAT 3' and 5' ATATACTTACTAAAATTAGCTTATATGGTTTCGCATATTGAGCAGCGTACGGATATCACCTA 3', were used to amplify *LEU2* from pOM13. Deletion of *MGM101* was confirmed by PCR amplification of the locus using the following primers: 5' CGAAATTTATCGACAGAATAATGG 3' and 5' GTRACTGACACTACGCACTACC 3'.

For each experiment needing *mgm101Δ rho⁰* cells, *MGM101* was freshly deleted to avoid further adaptation of *rho⁰* cells during normal handling, passage and subculturing. Likewise, new EtBr-generated *rho⁰* cells were generated for each experiment. *SIR3* was deleted from BY4741 using the following primers: 5' TTAGAAAGTTGTTTTGTTCTAACCAATTGGATTAGCTAAATGCAGGTGCGACAACCCCTTAAT 3' and 5' CATAGGCATATCTATGGCGGAAGTGAAAATGAATGTTGGTGGGCAGCGTACGGATATCACCTA 3' to amplify *URA3* from pOM12. Deletion of *SIR3* was confirmed by PCR amplification of the locus using primers 5' CACATAAGCAGCCCTTTCATC 3' and 5' GAATACAGAAGAGACTGCATG 3'.

Colony size determination

Yeast from the indicated colony type (*rho⁰* strains obtained by EtBr treatment, or subcultured adapted or UA colonies from parental *rho⁰* strains) were diluted and spread on YPD plates to generate single colonies. After 5 d of growth at 30°C, single colonies were imaged using a ChemiDoc MP (Bio-Rad). Images were processed with the open-source colony counting software OpenCFU to automatically count and measure the size of each colony (Geissmann, 2013). False-positive colonies resulting from noise were automatically removed by applying a -1 filter or manually removed from analysis. Colonies of area $< 0.72 \text{ mm}^2$ (100 pixels) were categorized as small/UA, while colonies of area $> 0.72 \text{ mm}^2$ were categorized as large/adapted.

Growth rates

Growth curves were measured using an automated plate reader (Tecan; Infinite M200, Research Triangle Park, NC). Each strain was grown to mid-log phase in rich, glucose-based media (YPD) and diluted to an OD₆₀₀ of 0.07 (2.0×10^6 cells/ml). A diluted strain of 10 μ l was added to a well containing 200 μ l YPD in a 96-well plate. Cells were propagated at 30°C without shaking, and an optical density at 600 nm (OD₆₀₀) was measured every 20 min for 72 h. For each strain, three independent colonies were tested in quadruplicate.

The maximum growth rate was calculated using the greatest change in OD₆₀₀ over a 240-min interval in 72 h.

Cell cycle assay

Cell cycle progression was assessed by measuring amount of DNA as described previously (Breedon, 1997; Fortuna *et al.*, 2001; Crider *et al.*, 2012). Mid-log phase yeast were synchronized by incubating cells with 10–100 μ M α -factor for 2.5 h on YPD with shaking at 30°C. Cells were released from arrest by washing with fresh YPD media and transferred to pheromone-free media. Cells were collected and fixed in 70% ethanol 0, 20, 40, 60, 80, 100, 120, 150, and 180 min after release from arrest. Cell cycle progression was assessed by measuring DNA content as described previously (Breedon, 1997; Fortuna *et al.*, 2001; Crider *et al.*, 2012). Briefly, cells were washed and digested with 250 μ g/ml RNase in sodium citrate buffer, pH 7.5, for 2 h at 50°C. After RNase digestion, cells were digested with 20 mg/ml Proteinase K for 2 h at 50°C. DNA was stained resuspending cells in citrate buffer containing 16 μ g/ml propidium iodide. DNA content was measured using a fluorescence-activated cell analyzer (LSRII, BD), and 50,000 events were recorded for each timepoint. The percentage of G₁, S, and G₂ phase cells was determined using FlowJo (FlowJo LLC, Ashland, OR).

RLS determination

RLS measurements were performed as described previously (Erjavec *et al.*, 2008) without alpha-factor synchronization. Frozen yeast strain stocks (stored at –80°C) were grown on YPD plates at 30°C, and rho⁰ cells were obtained by ethidium bromide treatment as previously described. Single colonies of each yeast strain were suspended in liquid YPD and grown at 30°C with shaking to mid-log phase (OD₆₀₀ 0.1–0.3). A 2- μ l aliquot of cell suspension was applied to a YPD plate. Small-budded cells were isolated and arranged in a matrix using a micromanipulator mounted on a dissecting microscope (Zeiss, Thornwood, NY, or Singer Instruments, Watchet, UK). When the small buds completed growth, their mother cells were removed and discarded, and the remaining daughter cells were named virgin mother cells. After each replication, the new bud was removed and discarded. This was continued until all replication ceased. The mean generation time and number of daughter cells produced by each virgin mother cell were recorded.

Assessing mitochondrial function using mitochondria-targeted roGFP

Mitochondrial redox state was measured as previously described in McFaline-Figueroa *et al.* (2011). Strains were transformed with a centromeric plasmid expressing mito-roGFP1 targeted to mitochondria using the ATP9 mitochondrial targeting sequence prior to EtBr treatment. After EtBr treatment as described previously, ~40–50 small rho⁰ colonies and ~8–10 large rho⁰ colonies were selected and grown for 12 h on selective media to obtain UA and A, respectively. These adapted cells were grown for another 24 h to obtain IAA. Images were acquired with an Axioskop 2 microscope equipped with a 100 \times /1.4 Plan-Apochromat objective (Zeiss, Thornwood, NY), an Orca-ER cooled CCD camera (Hamamatsu), and a pE-4000 LED illumination system (coolLED, Andover, UK). Images were acquired using NIS Elements 4.60 Lambda software (Nikon, Melville, NY). Oxidized and reduced channels were excited using a 365-nm LED and a 470-nm LED with a ET470/40 \times filter, respectively. All channels were acquired with a modified GFP filter (Zeiss filter 46 HE without excitation filter, dichroic FT 515, emission 535/30). Images were deconvolved using 60 iterations (100% confidence criterion) of a

constrained iterative restoration algorithm and a theoretical PSF based on a 507-nm emission wavelength using Volocity 6.3 (Perkin-Elmer, Waltham, MA). The reduced:oxidized ratio channel was calculated by dividing the intensity of the reduced channel (λ_{ex} = 470 nm, λ_{em} = 525 nm) by the intensity of the oxidized channel (λ_{ex} = 365 nm, λ_{em} = 525 nm) after background subtraction and thresholding for each channel individually.

RNA sequencing

Transcriptome was analyzed as previously described in Vevea *et al.* (2015). RNA was extracted from mid-log phase A and UA rho⁰ yeast cells using the RNeasy kit (Qiagen, Germantown, MD). RNA quality was analyzed with Agilent 2100 Bioanalyzer using a Plant RNA Nano chip, and only RNA samples with RNA Integrity Number (RIN) scores >9 were used for subsequent RNA-Seq. The mRNA library was generated using Illumina TruSeq RNA prep kit after poly-A pull-down enrichment of mRNA from total RNA samples. RNA-Seq was performed on an Illumina HiSeq2500 generating 200 million 100-base pair single-end reads per lane, with 10 samples multiplexed per lane (average 30 million raw reads per sample) by the Columbia Genome Center. Data were analyzed using Tophat, Cufflinks, and Cuffdiff protocol as described on the Galaxy platform (Afgan *et al.*, 2016). Differential expression was analyzed with DESeq2, an open-source differential gene expression analysis based on the negative binomial distribution (Love *et al.*, 2014). Differentially expressed genes were then analyzed using Funspec to group the large sets of up-regulated and down-regulated genes into gene ontology (GO) terms (Robinson *et al.*, 2002).

cDNA synthesis and quantitative PCR

RNA was extracted from mid-log phase UA and A rho⁰ cells using the RNeasy kit (Qiagen, Germantown, MD). RNA quality was analyzed as previously described and only RNA samples with RIN scores >9 were used for subsequent RT-PCR analysis. Genomic DNA contamination was removed from RNA samples with TURBO DNA-free Kit (Ambion, Carlsbad, CA). DNA-free RNA (1 μ g) was used for cDNA synthesis performed with SuperScript IV First-Strand Synthesis System (Invitrogen, Waltham, MA). cDNA was diluted and used for quantitative PCR with PowerUp SYBR Green Master Mix (Applied Biosystems, Carlsbad, CA) for adapted, superadapted, and UA samples. Primers for qPCR were designed with NCBI Primer Blast (www.ncbi.nlm.nih.gov/tools/primer-blast/) with a PCR product size of 100 base pairs and max T_m difference of 2°C. Primer specificity and amplification efficiency for each primer set were validated with a standard curve. *ACT1* was amplified with 5' TCGCCTTGACTTC-GAACAA 3' and 5' CAAAGCTTCTGGGGCTCTGA 3', *ADE17* with 5' CGTGACGCTGGTTTTCCAAT 3' and 5' CACCATGAACG-GCAGGATGT 3', *HSP30* with 5' GCTACGACGATGTGGAAGA 3' and 5' CAGGTTTCGGGTCGTGGATT 3', *PAU24* with 5' GGTATT-GCCCCAGACCAAGT 3' and 5' GCACTAGAGATGGCTGGCTT 3', *DAN1* with 5' GTA CTGACAGCACCGTCACA 3', and 5' GCTTTG-GAGGAGACTGGCTT 3' and *FIT3* with 5' TTGTCTGGACTGGT-GAAGGC 3' and 5' GTGGTTGCAGTGGTTGAAGC 3'. For each specified gene, Δ CT was calculated as CT_{target gene}–CT_{actin}, while fold change was calculated as 2^{– Δ CT} with actin serving as the endogenous control for each sample. For each gene-sample pair, a no-template control and nonreverse-transcriptase control were performed to control for genomic DNA contamination.

To determine the silencing rate, RNA was extracted from the same mid-log phase cells treated with EtBr for 3 and 5 d and analyzed by RT-qPCR. The silencing rate is calculated as the changes of the Δ CT between 3 and 5 d.

DHE superoxide staining

Mitochondrial superoxide was visualized by staining live cells with DHE as previously described in McFaline-Figueroa *et al.* (2011). Mid-log yeast cells propagated on SC liquid medium were incubated with 40 μM DHE dissolved in DMSO (Molecular Probes, Eugene, OR) for 30 min at 30°C, washed 2x with SC, and imaged without fixation (McFaline-Figueroa *et al.*, 2011). DHE was excited using a 561-nm LED and imaged with the microscope previously described with a dual eGFP/mCherry cube (59222; Chroma, Bellows Falls, VT). DHE images were deconvolved using 60 iterations (100% confidence criterion) of a constrained iterative restoration algorithm and a theoretical PSF based on a 610-nm emission wavelength using Volocity 6.3.

Statistical methods and data representation

All data were analyzed for normal distribution with the D'Agostino and Pearson normality test. The p values for simple two-group comparison were determined with a two-tailed Student's t test for parametric distributions and a Mann-Whitney test for nonparametric data. For multiple group comparisons, p values were determined with a one-way analysis of variance (ANOVA) with Tukey's post-hoc test for parametric distributions and Kruskal-Wallis test with Dunn's test-hoc test for nonparametric distributions. The Log-rank (Mantel-Cox) test was used to test statistical significance between RLS survival curves. GraphPad Prism7 (GraphPad Software) was used to conduct all statistical analysis and to create all graphs. Bar graphs show the mean and SEM; in box and whiskers graphs, the box represents the middle quartile, the midline represents the median, and whiskers show the minimum and maximum values. For RLS graphs, survival graphs are shown where the remaining percentage of viable cells is plotted over generation number. For all tests, p values are classified as follows: * $p < 0.05$, ** $p < 0.01$, *** $p < 0.001$, **** $p < 0.0001$, unless otherwise noted in the figure legends.

ACKNOWLEDGMENTS

We thank the members of the Pon laboratory for valuable discussion and critical review of the manuscript. This work was supported by grants from the National Institutes of Health: GM45735, GM122589, and AG051047 to L.P.; GM007367 and AR070013 to E.J.G.; AG055326 to C.N.S.; and AG053023 to R.H.-S.

REFERENCES

- Ai W, Bertram PG, Tsang CK, Chan TF, Zheng XF (2002). Regulation of subtelomeric silencing during stress response. *Mol Cell* 10, 1295–1305.
- Afgan E, Baker D, van den Beek M, Blankenberg D, Bouvier D, Cech M, Chilton J, Clements D, Coraor N, Eberhard C, *et al.* (2016). The Galaxy platform for accessible, reproducible and collaborative biomedical analyses: 2016 update. *Nucleic Acids Res* 44, W3–w10.
- Altaf M, Utley RT, Lacoste N, Tan S, Briggs SD, Cote J (2007). Interplay of chromatin modifiers on a short basic patch of histone H4 tail defines the boundary of telomeric heterochromatin. *Mol Cell* 28, 1002–1014.
- Breeden LL (1997). α -Factor synchronization of budding yeast. *Methods Enzymol* 283, 332–342.
- Chen XJ, Guan MX, Clark-Walker GD (1993). MGM101, a nuclear gene involved in maintenance of the mitochondrial genome in *Saccharomyces cerevisiae*. *Nucleic Acids Res* 21, 3473–3477.
- Contamine V, Picard M (2000). Maintenance and integrity of the mitochondrial genome: a plethora of nuclear genes in the budding yeast. *Microbiol Mol Biol Rev* 64, 281–315.
- Crider DG, Garcia-Rodriguez LJ, Srivastava P, Peraza-Reyes L, Upadhyaya K, Boldogh IR, Pon LA (2012). Rad53 is essential for a mitochondrial DNA inheritance checkpoint regulating G1 to S progression. *J Cell Biol* 198, 793–798.
- Dang W, Steffen KK, Perry R, Dorsey JA, Johnson FB, Shilatifard A, Kaeberlein M, Kennedy BK, Berger SL (2009). Histone H4 lysine-16 acetylation regulates cellular lifespan. *Nature* 459, 802–807.
- Di Gianvito P, Tesnière C, Suzzi G, Blondin B, Tofalo R (2017). FLO5 gene controls flocculation phenotype and adhesive properties in a *Saccharomyces cerevisiae* sparkling wine strain. *Sci Rep* 7, 10786.
- Dirick L, Bendris W, Loubiere V, Gostan T, Gueydon E, Schwob E (2014). Metabolic and environmental conditions determine nuclear genomic instability in budding yeast lacking mitochondrial DNA. *G3 (Bethesda)* 4, 411–423.
- Dunn CD, Jensen RE (2003). Suppression of a defect in mitochondrial protein import identifies cytosolic proteins required for viability of yeast cells lacking mitochondrial DNA. *Genetics* 165, 35–45.
- Dunn CD, Lee MS, Spencer FA, Jensen RE (2006). A genomewide screen for petite-negative yeast strains yields a new subunit of the i-AAA protease complex. *Mol Biol Cell* 17, 213–226.
- Ellahi A, Thurtle DM, Rine J (2015). The chromatin and transcriptional landscape of native *saccharomyces cerevisiae* telomeres and subtelomeric domains. *Genetics* 200, 505–521.
- Erjavec N, Cvijovic M, Klipp E, Nystrom T (2008). Selective benefits of damage partitioning in unicellular systems and its effects on aging. *Proc Natl Acad Sci USA* 105, 18764–18769.
- Fortuna M, João Sousa M, Côrte-Real M, Leão C, Salvador A, Sansonetty F (2001). Cell cycle analysis of yeasts. In: *Current Protocols in Cytometry*, New York: John Wiley & Sons.
- Fox TD, Folley LS, Mulero JJ, McMullin TW, Thorsness PE, Hedin LO, Costanzo MC (1991). Analysis and manipulation of yeast mitochondrial genes. *Methods Enzymol* 194, 149–165.
- Gauss R, Trautwein M, Sommer T, Spang A (2005). New modules for the repeated internal and N-terminal epitope tagging of genes in *Saccharomyces cerevisiae*. *Yeast* 22, 1–12.
- Geissmann Q (2013). OpenCFU, a new free and open-source software to count cell colonies and other circular objects. *PLoS One* 8, e54072.
- Gottschling DE, Aparicio OM, Billington BL, Zakian VA (1990). Position effect at *S. cerevisiae* telomeres: reversible repression of Pol II transcription. *Cell* 63, 751–762.
- Grunstein M (1997). Molecular model for telomeric heterochromatin in yeast. *Curr Opin Cell Biol* 9, 383–387.
- Hanson GT, Aggeler R, Oglesbee D, Cannon M, Capaldi RA, Tsien RY, Remington SJ (2004). Investigating mitochondrial redox potential with redox-sensitive green fluorescent protein indicators. *J Biol Chem* 279, 13044–13053.
- Higuchi R, Vevea JD, Swayne TC, Chojnowski R, Hill V, Boldogh IR, Pon LA (2013). Actin dynamics affect mitochondrial quality control and aging in budding yeast. *Curr Biol* 23, 2417–2422.
- Kaeberlein M, Hu D, Kerr EO, Tsuchiya M, Westman EA, Dang N, Fields S, Kennedy BK (2005). Increased life span due to calorie restriction in respiratory-deficient yeast. *PLOS Genet* 1, e69.
- Khrapko K, Kraysberg Y, de Grey AD, Vijg J, Schon EA (2006). Does premature aging of the mtDNA mutator mouse prove that mtDNA mutations are involved in natural aging? *Aging Cell* 5, 279–282.
- King MP, Attardi G (1989). Human cells lacking mtDNA: repopulation with exogenous mitochondria by complementation. *Science* 246, 500–503.
- Kirchman PA, Kim S, Lai CY, Jazwinski SM (1999). Interorganellar signaling is a determinant of longevity in *Saccharomyces cerevisiae*. *Genetics* 152, 179–190.
- Kozak ML, Chavez A, Dang W, Berger SL, Ashok A, Guo X, Johnson FB (2010). Inactivation of the Sas2 histone acetyltransferase delays senescence driven by telomere dysfunction. *EMBO J* 29, 158–170.
- Kujoth GC, Hiona A, Pugh TD, Someya S, Panzer K, Wohlgemuth SE, Hofer T, Seo AY, Sullivan R, Jobling WA, *et al.* (2005). Mitochondrial DNA mutations, oxidative stress, and apoptosis in mammalian aging. *Science* 309, 481–484.
- Longtine MS, McKenzie A 3rd, Demarini DJ, Shah NG, Wach A, Brachat A, Philippsen P, Pringle JR (1998). Additional modules for versatile and economical PCR-based gene deletion and modification in *Saccharomyces cerevisiae*. *Yeast* 14, 953–961.
- Love MI, Huber W, Anders S (2014). Moderated estimation of fold change and dispersion for RNA-seq data with DESeq2. *Genome Biol* 15, 550.
- MacLean M, Harris N, Piper PW (2001). Chronological lifespan of stationary phase yeast cells; a model for investigating the factors that might influence the ageing of postmitotic tissues in higher organisms. *Yeast* 18, 499–509.
- McFaline-Figueroa JR, Vevea J, Swayne TC, Zhou C, Liu C, Leung G, Boldogh IR, Pon LA (2011). Mitochondrial quality control during inheritance is associated with lifespan and mother-daughter age asymmetry in budding yeast. *Aging Cell* 10, 885–895.

- Mecocci P, MacGarvey U, Kaufman AE, Koontz D, Shoffner JM, Wallace DC, Beal MF (1993). Oxidative damage to mitochondrial DNA shows marked age-dependent increases in human brain. *Ann Neurol* 34, 609–616.
- Melov S, Hinerfeld D, Esposito L, Wallace DC (1997). Multi-organ characterization of mitochondrial genomic rearrangements in ad libitum and caloric restricted mice show striking somatic mitochondrial DNA rearrangements with age. *Nucleic Acids Res* 25, 974–982.
- Melov S, Schneider JA, Coskun PE, Bennett DA, Wallace DC (1999). Mitochondrial DNA rearrangements in aging human brain and in situ PCR of mtDNA. *Neurobiol Aging* 20, 565–571.
- Melov S, Shoffner JM, Kaufman A, Wallace DC (1995). Marked increase in the number and variety of mitochondrial DNA rearrangements in aging human skeletal muscle. *Nucleic Acids Res* 23, 4122–4126.
- Mortimer RK, Johnston JR (1959). Life span of individual yeast cells. *Nature* 183, 1751–1752.
- Muller-Hocker J (1989). Cytochrome-c-oxidase deficient cardiomyocytes in the human heart—an age-related phenomenon. A histochemical ultracytochemical study. *Am J Pathol* 134, 1167–1173.
- Muller-Hocker J (1990). Cytochrome c oxidase deficient fibres in the limb muscle and diaphragm of man without muscular disease: an age-related alteration. *J Neurol Sci* 100, 14–21.
- Muller-Hocker J, Schneiderbanger K, Stefani FH, Kadenbach B (1992). Progressive loss of cytochrome c oxidase in the human extraocular muscles in ageing—a cytochemical-immunohistochemical study. *Mutat Res* 275, 115–124.
- Nagley P, Linnane AW (1970). Mitochondrial DNA deficient petite mutants of yeast. *Biochem Biophys Res Commun* 39, 989–996.
- Park CB, Larsson NG (2011). Mitochondrial DNA mutations in disease and aging. *J Cell Biol* 193, 809–818.
- Park Y, Lustig AJ (2000). Telomere structure regulates the heritability of repressed subtelomeric chromatin in *Saccharomyces cerevisiae*. *Genetics* 154, 587–598.
- Pegg AE, Michael AJ (2010). Spermine synthase. *Cell Mol Life Sci* 67, 113–121.
- Renauld H, Aparicio OM, Zierath PD, Billington BL, Chhablani SK, Gottschling DE (1993). Silent domains are assembled continuously from the telomere and are defined by promoter distance and strength, and by SIR3 dosage. *Genes Dev* 7, 1133–1145.
- Rider JE, Hacker A, Mackintosh CA, Pegg AE, Woster PM, Casero RA Jr (2007). Spermine and spermidine mediate protection against oxidative damage caused by hydrogen peroxide. *Amino Acids* 33, 231–240.
- Robinson MD, Grigull J, Mohammad N, Hughes TR (2002). FunSpec: a web-based cluster interpreter for yeast. *BMC Bioinformatics* 3, 35.
- Rusche LN, Kirchmaier AL, Rine J (2003). The establishment, inheritance, and function of silenced chromatin in *Saccharomyces cerevisiae*. *Annu Rev Biochem* 72, 481–516.
- Schroeder EA, Raimundo N, Shadel GS (2013). Epigenetic silencing mediates mitochondria stress-induced longevity. *Cell Metabolism* 17, 954–964.
- Senapin S, Chen XJ, Clark-Walker GD (2003). Transcription of TIM9, a new factor required for the petite-positive phenotype of *Saccharomyces cerevisiae*, is defective in *spt7* mutants. *Curr Genet* 44, 202–210.
- Shampay J, Szostak JW, Blackburn EH (1984). DNA sequences of telomeres maintained in yeast. *Nature* 310, 154–157.
- Sherman F (2002). Getting started with yeast. *Methods Enzymol* 350, 3–41.
- Slonimski PP, Perrodin G, Croft JH (1968). Ethidium bromide induced mutation of yeast mitochondria: complete transformation of cells into respiratory deficient non-chromosomal “petites.” *Biochem Biophys Res Commun* 30, 232–239.
- Trifunovic A, Wredenberg A, Falkenberg M, Spelbrink JN, Rovio AT, Bruder CE, Bohlooly YM, Gidlöf S, Oldfors A, Wibom R, et al. (2004). Premature ageing in mice expressing defective mitochondrial DNA polymerase. *Nature* 429, 417–423.
- Trounce I, Byrne E, Marzuki S (1989). Decline in skeletal muscle mitochondrial respiratory chain function: possible factor in ageing. *Lancet* 1, 637–639.
- Veatch JR, McMurray MA, Nelson ZW, Gottschling DE (2009). Mitochondrial dysfunction leads to nuclear genome instability via an iron-sulfur cluster defect. *Cell* 137, 1247–1258.
- Vermulst M, Bielas JH, Kujoth GC, Ladiges WC, Rabinovitch PS, Prolla TA, Loeb LA (2007). Mitochondrial point mutations do not limit the natural lifespan of mice. *Nat Genet* 39, 540–543.
- Vevea JD, Garcia EJ, Chan RB, Zhou B, Schultz M, Di Paolo G, McCaffery JM, Pon LA (2015). Role for lipid droplet biogenesis and microlipophagy in adaptation to lipid imbalance in yeast. *Dev Cell* 35, 584–599.
- Wallace DC (2005). A mitochondrial paradigm of metabolic and degenerative diseases, aging, and cancer: a dawn for evolutionary medicine. *Annu Rev Genet* 39, 359–407.
- Walmsley RW, Chan CS, Tye BK, Petes TD (1984). Unusual DNA sequences associated with the ends of yeast chromosomes. *Nature* 310, 157–160.
- Wellinger RJ, Zakian VA (1989). Lack of positional requirements for autonomously replicating sequence elements on artificial yeast chromosomes. *Proc Natl Acad Sci USA* 86, 973–977.
- Woo DK, Poyton RO (2009). The absence of a mitochondrial genome in *rho0* yeast cells extends lifespan independently of retrograde regulation. *Exp Gerontol* 44, 390–397.